ACCSCIENCE PUBLISHING

International Journal of Bioprinting

RESEARCH ARTICLE

Development of an *in situ* 3D bioprinting and laser-assisted wound care model: From leech regeneration to space medicine applications

Giada Loi[1], Mariagrazia Zaccara[1], Francesca Cialdai[2], Chiara Risaliti[2], Glenda Leggieri[2], Lorenzo Notari[2], Daniele Bani[3], Michele Conti[1,4*], and Monica Monici[2]

[1] Department of Civil Engineering and Architecture, University of Pavia, Pavia, Italy

[2] ASA campus Joint Laboratory, ASA Research Division, Department of Experimental and Clinical Biomedical Sciences "Mario Serio", University of Florence, Florence, Italy

[3] Department of Experimental and Clinical Medicine, University of Florence, Florence, Florence, Italy

[4] 3D and Computer Simulation Laboratory, IRCCS Policlinico San Donato, San Donato Milanese, Milan, Italy

(This article belongs to the *Special Issue*: *Emerging Bioprinting Techniques for Regenerative Medicine*)

Abstract

Wound healing is a complex process that ensures tissue recovery and survival, but remains challenging to manage, particularly in deep wounds and burns. Conventional treatments require specialized operators, repeated interventions, and high costs. In extreme environments, such as space, the absence of dedicated facilities and personnel further complicates wound care, highlighting the need for novel, automated, and easy-to-use therapeutic strategies. In this study, we developed and validated a protocol that combines *in situ* 3D bioprinting with near-infrared (NIR) laser irradiation to promote graft integration and accelerate wound repair. The approach was tested in the leech model of a skin wound with tissue loss, selected for its suitability in reproducing key aspects of tissue regeneration and for its relevance in space-oriented regenerative medicine experiments design comprised four steps: (i) identification of biomaterial inks compatible with the wound environment; (ii) application of an optimized *in situ* 3D bioprinting protocol; (iii) NIR laser irradiation to stimulate graft integration; and (iv) histological and immunofluorescence evaluation of healing outcomes compared to controls (bioprinting only, laser only, and untreated). Results demonstrated that the integrated protocol significantly improved wound healing, preventing fibrosis and enhancing re-epithelialization, fibroblast activation, and transdifferentiation. The combined treatment outperformed all control conditions, confirming the synergistic effect of *In situ* bioprinting and laser irradiation. This work introduces an advanced wound care strategy integrating biofabrication and photobiomodulation. The protocol shows high potential for clinical translation, with applications not only in conventional medical settings but also in extreme environments such as space.

Keywords: 3D *In situ* bioprinting; Wound healing; Near-infrared laser therapy; *In vivo* model

***Corresponding author:**
Michele Conti
(michele.conti@unipv.it)

Citation: Loi G, Zaccara M, Cialdai F, *et al.* Development of an *In situ* 3D bioprinting and laser-assisted wound care model: From leech regeneration to space medicine applications. *Int J Bioprint*. 2026;12(1):637-655. doi: 10.36922/IJB025400406

Received: September 29, 2025
Revised: December 5, 2025
Accepted: December 8, 2025
Published online: December 19, 2025

1. Introduction

Wound healing is a highly conserved biological process that allows organisms to survive injuries. It is conventionally divided into three phases, namely inflammation, proliferation, and remodeling. However, it would be more accurate to define it as a set of complex mechanisms that follow one another and partially overlap within a defined timeline. Wound healing of the skin involves several cell types, including immune cells, fibroblasts, endothelial cells, and keratinocytes, whose activity is tightly regulated by a number of biochemical and mechanical factors.[1,2]

Among the cell populations involved in the healing process, fibroblasts play a pivotal role as they take part in all stages, orchestrating the activities of other cell populations by producing numerous soluble factors and mediating cell–cell cross-talk. During the inflammatory response to tissue injury, activated fibroblasts (stromal activation) promote events that occur during the proliferation phase, such as re-epithelialization and neoangiogenesis. Then, they transdifferentiate into myofibroblasts, capable of regulating connective tissue remodeling and wound closure by combining extracellular matrix (ECM) biosynthesis and intrinsic contractile properties through the development of an extended myofilament cytoskeleton.[3]

When the normal progression of one or more events leading to healing is altered quantitatively, qualitatively, or temporally, the whole process is impaired. The consequences of wound healing dysfunction range from healing delay and keloid scarring to much more severe and chronic conditions, such as chronic ulcers and fibrosis.[4,5] The management of healing dysfunction is an unmet clinical and socio-economic need. Reports on chronic wounds and their burden on national health systems show that in the United States (US), approximately 10 million patients (2.5% of the US population) are affected by chronic ulcers, with a significant impact on their quality of life and associated costs exceeding 20 billion dollars.[6] Similar numbers have been reported for other countries. Moreover, the prevalence of healing disorders is expected to increase further due to the aging population, rising diabetes and obesity, and the persistent problem of infections and antibiotic resistance.[7,8] All these reports indicate that one of the most effective ways to improve patients' quality of life and reduce the social costs of defective healing is to enhance wound care and prevent infections and wound-healing complications.

The management and care of severe wounds and burns are difficult and require precise wound diagnostics and complex therapeutic strategies aimed at promoting wound closure, including wound debridement, cleaning and disinfection, infection prevention, appropriate dressing, and pharmacological and non-pharmacological treatments, such as laser therapy and negative pressure therapy. When surgery is needed to merge the wound edges, remove the necrotic tissue, or prepare and apply a skin graft, as occurs in deep burn injuries, specialist intervention is required.[9,10]

Wound management and therapy are more complicated in extreme environments on Earth and in space, where hospital centers with adequate facilities, instruments, and skilled operators are lacking. Moreover, in extreme environments, the resilience of the organism to injury can be undermined by environmental stressors. During spaceflight, microgravity, radiation, and other stress factors induce significant pathophysiological alterations that could affect the efficiency of the healing process.[11–13] Therefore, it is necessary to make further efforts to search for new therapeutic strategies that are effective and also meet the requirements to be applied in extreme environments. In cases of severe injuries, ulcers, and burns, the aim is to automate and simplify medical and surgical procedures and to develop strategies that promote tissue regeneration. Substantial expectations are placed on the development of skin analogues that can mimic specific morpho-functional characteristics of the skin. These tissue analogues have several advantages: they allow the skin barrier to be rapidly restored, avoiding the need for cadaveric or heterologous transplants at risk of rejection and the removal of autologous skin flaps from the patient. Moreover, in the future, automated facilities could enable the preparation of tissue analogues even in extreme environments.[14]

Although it is complicated to recreate the morpho-functional complexity of the skin, interesting advances have recently been made in 3D bioprinting and tissue engineering techniques. Space agencies are developing systems for 3D bioprinting on board spacecraft or space stations, and one such facility has already been installed on the International Space Station (ISS).[15] These techniques could play a significant role in managing medical emergencies that may occur during future space exploration missions, in which, given the distance from Earth, an emergency medical evacuation with return to our planet would not be possible.

This study aims to develop a wound care model that, while accounting for the constraints and requirements imposed by extreme environments, can serve as a solid starting point for future wound management strategies in these settings. In particular, the protocol studied for the management of wounds with loss of substance consists of *in situ* 3D bioprinting a tissue construct (graft) using a biocompatible ink embedding human dermal fibroblasts, followed by the application of a near-infra red (NIR) laser source.

The wound care protocol was tested in an *in vivo* model of a wound with loss of substance in the leech. This invertebrate represents a fascinating model for studying wound healing and tissue regeneration[16-19] because its sequence of events leading to healing is highly similar to that of vertebrates. This is a remarkable example of the evolutionary conservation of critical physiological functions.[16] In addition to being a recognized model of wound healing, the leech was selected for its ease of management, including in future experiments on space platforms[20] and other extreme environments, due to its minimal husbandry requirements for long-term survival.

Although wound healing in *Hirudo verbana* proceeds faster than in humans, the sequence of events is conserved. Inflammatory cell recruitment and fibroblast activation occur within 24–48 h, followed by early collagen deposition within 3–5 days.[16] In the leech, healing relies on re-epithelialization and ECM remodeling, making its evolution comparable to human regenerative mechanisms despite the shorter timescale.

In designing this wound care protocol, two advantages were hypothesized: (i) the 3D bioprinting of the graft directly in the wound bed (*in situ*) would have immediately closed the dead space, temporarily replacing the skin barrier and protecting the integrity of the body from the external environment; (ii) the NIR laser radiation, modulating inflammation and stimulating tissue repair mechanisms, would have promoted the integration of the graft with the surrounding tissue, speeding up the wound healing process.

It is noteworthy that both *in situ* bioprinting and laser technologies can be automated, and the relatively small size of the instrumentation makes them suitable for use even in extreme environments, provided they are made compliant with the requirements for operating in such conditions.

2. Materials and Methods

2.1. Study design

The study involved the following steps (Figure 1):

(i) Preparation of the *in vivo* wound model through surgical removal of dorsal tegument tissues.

(ii) Pre-printing activities, which consisted of the selection, preparation, and testing of fibroblast-enriched bioinks compatible with the wound environment. They also involved the development and validation of a setting for *in situ* 3D bioprinting through monolayer, multilayer, and leech phantom tests.

(iii) Printing through the application of the developed *in situ* 3D bioprinting protocol in the model of a wound with loss of substance in the leech.

(iv) Treatment with an NIR dual-wavelength laser source to promote the integration of the graft into the surrounding tissues and shorten healing times.

(v) Post-care analysis through histology and immunofluorescence to evaluate graft integration and wound healing.

2.2. Preparation of the wound model with loss of substance in the leech

Leeches (*H. verbana*; Phylum: Annelida, Subclass: Hirudinea) about 6 cm long and 0.7 cm in diameter were purchased from Ricarimpex (Eysines, France). Since leeches are invertebrates, Animal Ethics Committee approval is not required for their use in research. However, in this study, the animals were treated in accordance with strict ethical principles to avoid suffering, and all procedures were performed under anesthesia.

The leeches were housed in aerated aquaria containing mineral water at about 20°C. Before surgical procedures, the leeches were anesthetized by immersion in a 10% ethanol solution (AppliChem GmbH, Germany).

An excised wound was created in the dorsal skin (at about the 14th metamere) of each leech with a surgical biopsy punch (Figure 1A). The original punch produced a cylindrical wound with a diameter of 3 mm and a depth of 7 mm. To avoid compromising the animal's internal organs and limit the excision to the skin (or integument) level, the punch was modified by an inner adapter to reduce the depth to 2 mm (Figure S8). The adapter was designed using the Autodesk Inventor CAD software (v.2023, Autodesk, Inc., US). It consisted of a hollow cylinder, 4 mm in diameter and 5.5 mm thick, suitable for insertion into the punch. The computer-aided design (CAD) model was exported as an STL file that was imported into Slic3r for printing. For this application, Nylon PA12 powder was used, and the 3D printing technology was binder jetting using an HP Multijet Fusion system (HP, US). The PA12 was selected due to its ability to be autoclaved (melting point of 220°C and autoclave temperature of 140°C). To create wounds, the punch was pressed and slightly rotated on the leech's back to cut and remove a circular skin biopsy. The wound was cylindrical, measuring 3 mm in diameter and 2 mm in depth.

2.3. Cell culture

Normal human dermal fibroblasts (nHDF) (ATCC, US) were cultured in Dulbecco's modified Eagle's medium (Sigma-Aldrich, Germany) supplemented with 10% fetal

bovine serum (Sigma-Aldrich, Germany), 100 IU/mL penicillin, 100 µg/mL streptomycin, and 2 mM glutamine (Sigma-Aldrich, Germany) at 37°C in a humidified atmosphere of 5% CO_2 in air.

2.4. Biomaterial ink selection and preparation

According to previous reports,[21-24] two different biomaterial inks suitable for inducing regeneration were preliminarily studied: one composed of alginate and gelatin (SA-GEL), and the other a commercial product (CELLINK Fibrin, see below).

2.4.1. Alginate and gelatin-based biomaterial ink

A hydrogel based on gelatin (GEL) and sodium alginate (SA) was prepared at a final concentration of 4% (w/v) and 8% (w/v), respectively, as described in previous papers.[22,25] First, the GEL powder (G9391, Sigma-Aldrich, Germany) was dissolved by vortexing in sterile phosphate-buffered solution (PBS) in a thermostatic bath and heated to +72°C. Then, SA powder (W201502, Sigma-Aldrich, Germany) was added to the GEL solution and vortex-mixed until completely homogenized. The hydrogel was centrifuged for 5 min at 2,000 rpm to remove air bubbles, then pasteurized in a thermostatic water bath at 72°C for 1 h. Finally, the hydrogel was transferred to a syringe and stored in a refrigerator at 4°C until use. All steps described were performed under sterile conditions.

2.4.2. Hydrogel

CELLINK Fibrin (IKC206000301, Sweden) is a commercially available nano-fibrillated cellulose (NFC)/alginate-fibrinogen-based hydrogel. The nanosized fibrils make the bioink semi-translucent, allowing cell imaging and analysis. Among the various biomaterials, fibrinogen-based hydrogels, extensively studied in the literature as biopolymers for tissue engineering applications, are particularly valued for their strong proangiogenic properties, outstanding biocompatibility and biodegradability, and customizable physicochemical characteristics.[26] This hydrogel offers significant advantages compared to other biomaterials, making it a highly suitable candidate for skin scaffold fabrication. In addition, the commercial kit includes an enhanced cross linking solution composed of an ionic binding agent ($CaCl_2$) to develop a compound network with improved printability and stability.

2.5. Preparation of the bioink containing human dermal fibroblasts

The bioink preparation was carried out under sterile conditions. After washing the cells with 5 mL of PBS, they were detached with 1 mL of trypsin and then centrifuged for 5 min at 1,200 rpm. The supernatant was discarded, and the cell pellet was resuspended in fresh culture medium at a final concentration of 3 $\times 10^7$/mL. The cell suspension was transferred into a syringe, which was then connected to a second syringe containing CELLINK Fibrin hydrogel, with a 1:10 ratio. The syringes were linked using a luer connector, and the bioink was prepared by passing the mixture between the two syringes until a visually uniform consistency was achieved (about eight passages). The bioink was then transferred to the printing cartridge, the needle was connected, and the cartridge was inserted into the printer head #1 (PH1).

2.6. Bioprinter

The 3D bioprinter used in this study is the Cellink INCREDIBLE+ (D16110010716, CELLINK, Sweden). This bioprinter features a pneumatic extrusion system with dual print heads (PHs), enabling the bioprinting of different types of cells and bioinks within the same structure without switching cartridges or pausing the process. PHs can be heated to 130°C, allowing the bioprinting of a wide range of biomaterials, from hydrogels (e.g., GEL, chitosan, hyaluronic acid, and alginate) to thermoplastic materials (e.g., polycaprolactone) and synthetic materials (such as Pluronic). PHs move along the x–y axes, while the print bed moves along the z-axis. The extrusion system consists of an external air compressor that generates an airflow in the cartridge–piston system, causing the material to extrude through the nozzle. The maximum pressure supported by the bioprinter is 700 kPa. The patented Clean Chamber Technology provides a sterile environment inside the bioprinter without the need for a laminar airflow hood. Moreover, behind the two PHs are two built-in UV light-emitting diodes with different wavelengths: 365 nm to sterilize the printing area and 405 nm to crosslink those hydrogels that require photo-crosslinking. Sterility was maintained using a high-efficiency H13 HEPA filter (retention rate > 99.95%) and a fan that creates positive air pressure inside the bioprinter chamber.

2.7. Setting for *in situ* bioprinting

To enable *in situ* 3D bioprinting, the first step involved generating a customized G-code. The purpose was to process an image of the printing plate and the cavity where printing would be performed to obtain a specific G-code. Three steps were employed to convert the acquired image to the final G-code. Different software was used for each step:

(i) Image segmentation with MATLAB (R2019b, MathWorks, US): The image was imported, segmented, and the coordinates of the wound area to be printed were extracted.

(ii) CAD model development with Autodesk Inventor: The CAD model was developed based on the

extracted wound coordinates, and the model was exported in STL format.

(iii) G-code generation with Repetier-Host (Hot-World GmbH & Co. KG, Germany) and Slic3r: The STL file was imported, and the printing options were set for the G-code generation. Before starting printing, the bioprinter settings were configured. The axes were homed, and the z-axis was calibrated. Finally, the correct printing pressure was set. PH1 was opened and, starting from 0 kPa, the pressure was gradually increased until the material was extruded.

2.7.1. Printing bed picture acquisition

Initially, a procedure for photographing the wounded leech on the printing plate was established. To outline the wound, we used a 3D-printed perforated disk that could be placed on the wound located on the leech's back. This disk, designed in Autodesk Inventor and printed in polylactic acid (PLA) using a fused deposition modeling 3D printer, had an inner diameter matching the wound diameter (3 mm), an outer diameter of 5 mm, and a height of 1 mm (Figure S1).

Then, a four-step procedure was followed for photographing (Figure 1B). First, the HEPA filter was removed from the top of the bioprinter. Second, using the bioprinter's Move axis function, the PHs were moved to the lowest coordinate on the x-axis and to the highest coordinate on the y-axis to frame the entire printing plate. Third, a digital camera was placed above the bioprinter to capture images of the whole printing plate. Finally, the photos were edited and cropped to the edges of the printing plate to segment and analyze only the objects of interest.

2.7.2. Image segmentation

In the second step, a code for image segmentation and processing was developed using MATLAB (Figure 1B) to obtain the coordinates of the wound outline on which bioprinting was to be performed. The procedure of image segmentation can be divided into the following five phases: image import, image binarization, selection of the contour pixel of interest, transformation of contour pixels into coordinates for 3D printing, and saving of the extracted coordinates in an XSLX format. To ensure high usability, an application based on the above-described steps was developed using MATLAB's App Designer. A summary of the MATLAB code's pseudocode is provided. More details on the MATLAB code are provided in **Section S1.2** and **Figures S2 and S3** in the **Supplementary Materials**.

```
# --- 1. Setup ---
clear_all()
close_all()
clc()
# --- 2. Load and preprocess image ---
picture = load_image('s_1.jpg')
image = extract_channel(picture, 'blue')
image = invert(image)
im_bw = binarize(image, threshold=0.5)
show(im_bw, title= 'Binarized image')
# --- 3. Find valid contours ---
all_contours = find_contours(im_bw)
B = [c for c in all_contours if size(c) > 20]
plot_contours(B, color= 'red', title= 'Contours')
# --- 4. Plate to real-world coordinates ---
plate = B[0]
plate_real_size = (128, 86) # mm (width, height)
pixel_bounds = get_bounds(plate)
scaling_x, scaling_y = compute_scaling
(pixel_bounds, plate_real_size)
x_plate, y_plate = convert_to_real(plate, pixel_bounds,
scaling_x, scaling_y)
plot(x_plate, y_plate, label= 'Plate')
# --- 5. Object transformation ---
coordinates = []
for obj in B[1:]:
    x_obj, y_obj = convert_to_real(obj, pixel_bounds,
    scaling_x, scaling_y)
    plot(x_obj, y_obj, label='Object')
    coordinates.append((x_obj, y_obj))
label_axes('x [mm]', 'y [mm]')
add_legend()
# --- 6. Export results ---
save_to_excel('s_1_0412.xlsx', coordinates)
```

2.7.3. CAD model development

The coordinates saved in the XLSX file, based on the printing plate coordinate system, were imported into Autodesk Inventor. Based on the shape given by the coordinates derived from the image, a 2D sketch was created and extruded. The CAD model was then exported as an STL file.

Table 1. Main printing parameters

Parameters	Value (mm)
Layer height	0.35
Default extrusion width	0.41
Bed size (x)	128
Bed size (y)	86
Origin (x)	63
Origin (y)	44

2.7.4. Option setting and G-code generation

A further step concerned the G-code generation and print settings (Figure 1B). Initially, the STL file was imported into Slic3r to set the printing parameters. The main parameters are summarized in Table 1, primarily the extrusion height (which defines the layer height), the extrusion width, and the printing bed dimensions and origins, which are necessary for correct printer calibration. Then, the G code was generated, and printing was started.

2.8. Software validation

Before using the above protocol in the animal model, it was optimized and validated in simpler scenarios using monolayer and multilayer assays and a surrogate animal model.

2.8.1. Monolayer assay

The monolayer validation replicated some flat geometrical shapes drawn on the printing plate. A picture of the shapes was taken and processed, following the protocol described in **Section 2.7**. Then, the printing was performed to verify the correct material deposition on the drawing. The procedure was optimized to correctly reproduce a rectangle, three straight lines, and a circle (Figure S4). In all these tests, the selected ink was the SA-GEL-based hydrogel.

2.8.2. Multilayer assay

The multilayer validation was performed by correctly depositing four layers of material within a support with a hole. The first one was a parallelepiped with dimensions 10× 10× 2 mm. In this case, a SA-GEL-based hydrogel was used as it is cross-linkable with a calcium chloride ($CaCl_2$)-based solution and extractable from the support to analyze the printed structure. Two different dyes were mixed with the hydrogel to verify the correct separation of the layers.

A second multilayer experiment was necessary to simulate the wound shape in the *in vivo* model. In particular, the correct gel deposition in a cylindrical model was evaluated. This cylinder-shaped hole had a diameter of 3 mm and a depth of 2 mm (Figure S5).

2.8.3. Leech phantom

Before being used on the actual animal model, the software was tested on a dummy model, termed "leech phantom" (Figure S6). It was made in ballistic GEL through a 3D-printed mold. The ballistic GEL was mixed with graphite, giving the phantom a black color, so that the surrogate animal model faithfully mimicked the actual

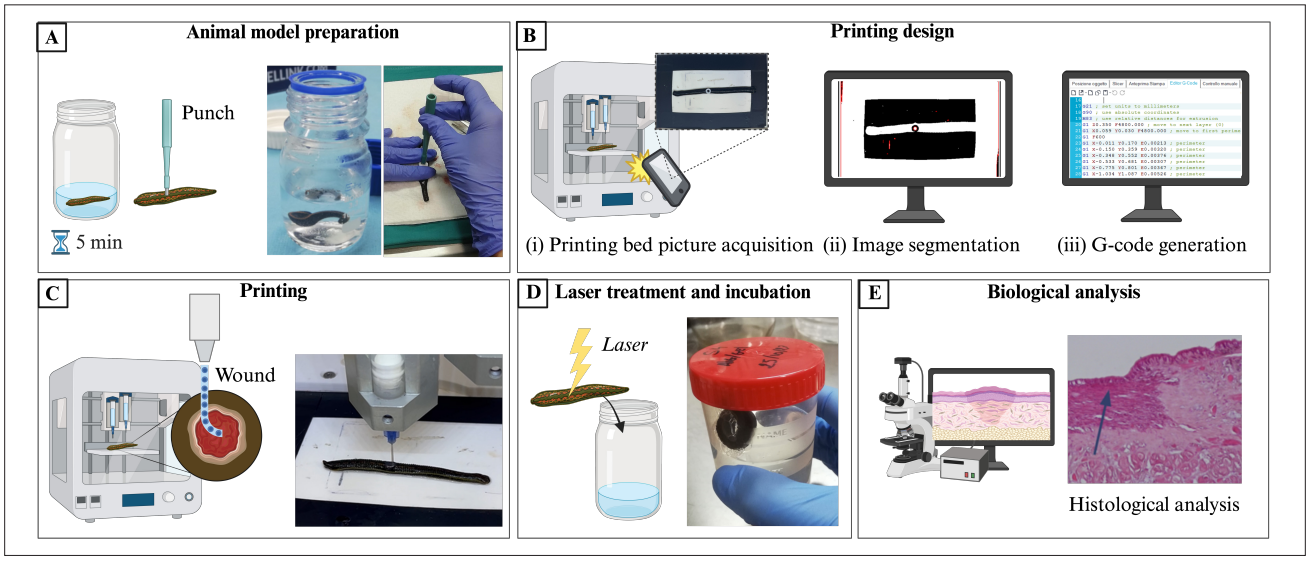

Figure 1. Schematic representation of the experimental procedures. (A) Animal model preparation. Leeches are anesthetized through immersion in 10% ethanol, and then a surgical tissue excision is made on the dorsal skin of each leech using a surgical biopsy punch. (B) Printing design. (i) Acquisition of digital images of the printing plate and the cavity to be filled by bioprinting. (ii) Image segmentation. (iii) G-code generation. (C) 3D printing of the bioink in the wound bed. (D) Laser treatment to promote graft integration, and incubation of the animals in separate aquarium boxes. (E) Post-treatment histological analyses.

wounded leech model. The mold was designed using a CAD model that reproduced the shape and dimensions of a leech with a cylindrical wound on the back. In particular, the phantom had a length of 6 cm and a diameter of 1 cm, whereas the wound had a diameter of 3 mm and a depth of 2 mm. The phantom was printed on a commercial FDM printer using PLA (Figure S7). The mold was first smeared with Vaseline for easy removal. Then, the ballistic GEL was melted and then poured into the mold. After 20 min of drying, the ready-to-use leech phantom was extracted from the mold. Initially, the wound was highlighted with white chalk to ease its identification by the software. Then, the leech phantom was placed on the printing plate, and a picture was taken. The above-described protocol was then applied: the software correctly elaborated the picture and generated the G-code for printing. In these tests, the SA-GEL-based hydrogel was employed.

2.9. *In situ* bioprinting in the *in vivo* model of wound with loss of substance in the leech

For the *in situ* bioprinting, anesthetized leeches were placed on the printing plate, and the procedure described in **Sections 2.7 and 2.8** was applied. Briefly, a circular-shaped object was put on the leech to highlight the wound, and a picture of the wounded leech on the printing plate was taken with a digital camera (Nikon D5200, Japan) (Figure S9A). The wound contour pixels were selected through the procedure developed in MATLAB (Figure S9B). The CAD model was designed in Autodesk Inventor for the extracted contours, and an STL file was generated (Figure S9 C). The STL file was imported into Slic3r, where the printing parameters were imposed, and the G-code was generated. Finally, the *in situ* 3D bioprinting into the wound was performed (Figures 1C and S9D). Immediately after printing, a $CaCl_2$ solution was added to the printed graft in the wound to crosslink the hydrogel for 3 min (Figure S9E). Before returning to water, the leeches were allowed to recover from anesthesia in a Petri dish with 5–6 mL of PBS for 5 min (Figure S9F). Then, each animal was placed in a separate small aquarium to prevent them from sticking to one another (Figure S9G).

The *in situ* 3D bioprinting procedure on the *in vivo* model was first validated using the SA-GEL hydrogel. On the other hand, the CELLINK Fibrin hydrogel containing human dermal fibroblasts was used for the final wound care protocol.

2.10. Near-infrared laser treatment

In this study, an NIR laser treatment was used to promote graft integration (Figure 1D). The laser source was a Multiwave Locked System laser (MLS-MiS; ASA S.r.l., Italy). It is a class IV NIR laser system with two synchronized sources. The first source is a pulsed laser diode emitting at 905 nm, with peak power ranging from 140 W ± 20% to 1 kW ± 20% and a pulse frequency of 1–2,000 Hz. The second source is a laser diode emitting at 808 nm wavelength that can operate in continuous (max power 6 W ± 20%) or frequency mode (pulse repetition rate 1–2,000 Hz, 50% duty cycle). The two laser beams work simultaneously and synchronously, with their propagation axes coincident.

Leeches were exposed to laser radiation every 24 h for four consecutive days, starting 24 h after the bioprinting procedure. To perform the laser treatment, the leech was placed in a plastic support, shaped like a half-tube, designed to securely and safely house a leech. The inner surface of the half-tube was smooth, facilitating gentle contact with the leech's skin and allowing it to extend comfortably along its length. The parameters used for the laser treatment were: frequency 10 Hz, intensity 50%, treatment time 10 s, and fluence 4.92 J/cm^2. The treatment parameters were chosen not only on the basis of the effects of laser treatment on fibroblasts, which have been extensively evaluated in previous studies on fibroblast cultures,[27-29] but also considering other aspects, such as the color of the animal's integument, the depth of treatment, and the duration of exposure based on the anesthesia given to the animal.

2.11. Tissue sampling, processing, and histological analysis

Six hours after the last MLS-MiS laser treatment, the leeches were anesthetized in a 10% ethanol solution. Once anesthetized, they underwent fixation by immersion in a fixative solution (ImmunoFix, phosphate-buffered, 4% paraformaldehyde, pH 7.4; Bio-Optica, Italy). The leeches were maintained in the fixative for 2 h at room temperature, then stored at 4°C for 48 h. The extremities of the animals were removed, preserving only the body segment that included the wound for dehydration in graded ethanol. Following dehydration, samples were cleared by two passages in Bio-Clear (Bio Optica, Italy), placed in paraffin oil, and finally embedded in paraffin wax (Bio-Optica, Italy) at 58°C overnight. Sections of 5-µm thickness were mounted on glass slides. Then, two histological staining were carried out (Figure 1E): (i) hematoxylin and eosin (H&E) to provide an overview of the general morphology and histological features; (ii) Picrosirius red staining (0.2% Picrosirius red solution for 60 min) to identify collagen fibers, which appear intensely red. The stained sections were dehydrated, cleared, and embedded in a permanent mounting resin under coverslips. Images of the stained sections were acquired using a Nikon DS F12 CCD camera (Japan) connected to a Nikon Eclipse E200 light microscope (Japan) at 4× and 20× magnification.

2.12. Collagen fiber morphometry

In each Picrosirius red-stained section, two photomicrographs of the connective tissue of the wound bed were taken at random using the Nikon DS F12 CCD camera connected to a Nikon Eclipse E200 light microscope at 40× magnification (each micrograph: 57,700 μm^2). On each image, four regions of interest (ROI), 10,000 μm^2 each, were randomly chosen: here, the surface area of the collagen fibers was selected by thresholding (to exclude the Picrosirius red-negative amorphous ground substance and cells) and measured using ImageJ 1.53k software (http://imagej.nih.gov/ij). Values are expressed as the percent area of collagen fibers over the whole ROI area.

2.13. Immunofluorescence analysis

Immunofluorescence staining was performed on 5 μm sections of the paraffin-embedded samples. After paraffin removal in Bio-Clear (Bio-Optica, Italy) and rehydration in graded ethanol, the sections were subjected to antigen retrieval by immersion in citrate buffer at 90°C for 10 min, followed by cooling to room temperature for 30 min. Then, after rinsing in isotonic PBS, the sections were incubated with 2 mg/mL glycine in PBS for 15 min and 5% bovine serum albumin (BSA) in PBS for 1 h to block non-specific antibody binding. A rabbit monoclonal anti- heat shock protein 47 (HSP47) immunoglobulin G (IgG) antibody (Millipore, US), diluted 1:50 in PBS + 3% BSA, was used to detect fibroblasts. A mouse monoclonal anti-alpha smooth muscle actin (α-SMA) IgG antibody (Millipore, US), diluted 1:100 in PBS + 3% BSA, was used to detect activated myofibroblasts. The slides were incubated with the primary antibodies at 4°C overnight, washed thoroughly with PBS, and incubated with the appropriate secondary antibodies: tetramethylrhodamine isothiocyanate (TRITC)-conjugated (red emission) goat anti-rabbit IgG (Millipore, US), diluted 1:100 in PBS + 3% BSA, to label HSP47 immunoreactivity; and fluorescein isothiocyanate (FITC)-conjugated (green emission) goat anti-mouse IgG (Millipore, US), diluted 1:200 in PBS + 3% BSA, to label α-SMA immunoreactivity. The secondary antibodies were incubated at room temperature for 2 h and then washed thoroughly in PBS. Finally, cell nuclei were counterstained with 4´,6-diamidino-2-phenylindole (DAPI) present in the mounting medium. Images were acquired using an Olympus BX63F fluorescence microscope (Japan).

2.14. Statistical analysis

Morphometric data are presented as means ± SD of the measurements of four individual animals, with four ROI (approximately 10,000 μm^2 each) per animal across the different experimental groups. Statistical comparison of differences between groups was performed using one-way analysis of variance (ANOVA) followed by Student's *t*- test for unpaired values, assuming $p \leq 0.05$ as significant. Calculations were performed using Prism 5.0 software (GraphPad Software, US). For immunofluorescence analysis, at least 10 random fields were scored per slide.

3. Results

3.1. Validation of the software for the 3D bioprinting protocol

Before employing the animal model, the developed protocol was tested and validated. First, tests on bioprinted monolayers were conducted. They consisted of replicating some planar geometrical shapes visible on the printing plate. These were digitally acquired and processed according to the developed protocol. Finally, the printing was made, and the correct material deposition on the drawing was verified. The procedure was optimized to correctly reproduce a rectangle, three separate straight lines, and a circle. Second, tests on bioprinted multilayers were performed to verify the correct deposition of four layers of bioink within a hole made into the supporting structure. The first 3D printout was a 10 ×10× 2 mm parallelepiped, while the second was a cylinder with a diameter of 3 mm and a depth of 2 mm, necessary to test conditions similar to those in the experimental tests with the animal model. The protocol successfully guaranteed the deposition of four layers of material in the correct coordinates. Finally, a test with a GEL-moulded leech phantom was performed to validate the software further. Initially, the wound was highlighted with white chalk to ease identification by the software. Then, the leech phantom was placed on the printing plate and processed according to the developed protocol, which successfully generated a conformal bio printed construct within the wound model created on the leech phantom.

3.2. Validation of the *in situ* 3D bioprinting procedure in the *in vivo* wound model

Two tests were conducted. The first was to validate the *in situ* 3D bioprinting procedure in the *in vivo* wound model, using the SA-GEL hydrogel bioink and the $CaCl_2$ crosslinking agent. The second aimed to validate the entire procedure using the more complex CELLINK Fibrin hydrogel bioink, with or without human dermal fibroblasts, and to optimize it for the wound care protocol. Again, $CaCl_2$ was used as a crosslinking agent. The fibrinogen-based hydrogel was chosen as a suitable environment for human dermal fibroblasts since, in previous experiments, it has been shown to preserve cell viability[26] and function better than the SA-GEL.[21] Human dermal fibroblasts were incorporated into the bioink to promote tissue repair, as they can release growth factors and cytokines that facilitate healing and enhance tissue regeneration.[30] Additionally, they can produce ECM components that

provide both structural support and biochemical signals essential for tissue repair.[31] Furthermore, fibroblasts can transdifferentiate into myofibroblasts, which play a critical role in the remodeling phase of wound healing by contributing to tissue contraction and ECM remodeling.[32]

For these tests, models of wounds with loss of substance were prepared in the leeches as described in **Section 2.2**. The animals (n=9) were then divided into three groups:

(i) Untreated animals (n=3), no *in situ* 3D bioprinting, served as a negative control.

(ii) Animals (n=3) that received an *in situ* 3D-bioprinted graft of SA-GEL hydrogel.

(iii) Animals (n=3) that received an *in situ* 3D-bioprinted graft of CELLINK Fibrin hydrogel containing human dermal fibroblasts.

The *in situ* 3D bioprinting procedure was successful with both the bioinks (SA-GEL and CELLINK Fibrin), as demonstrated by their precise deposition within the wounds and the stability of the grafts. The animals were monitored before and after receiving the *in situ* 3D-bioprinted grafts, and the results were compared with untreated wounded controls. Visual inspection did not reveal any adverse effects of the bioprinting procedure.

The next step was to analyze histologically the grafts in the wound beds and surrounding tissues taken 4 days after *in situ* bioprinting, and to compare them with the untreated wounds. Examination of the H&E-stained sections from the untreated controls (Figure 2A) showed a wound healing process at a very early stage: the surface epithelium was particularly thin, and the underlying connective tissue appeared as a loose meshwork containing a few cells and was distinct from the surrounding tissues (as shown in the inset). The sections from the leeches that received the SA-GEL graft (Figure 2B) showed a thin epithelial layer covering the whole graft, and the bioprinted graft appeared as a dense fibrous layer containing scattered cells and adhering firmly to the surrounding tissues. The sections from the leeches grafted with the CELLINK Fibrin hydrogel containing human dermal fibroblasts (Figure 2C) showed a thicker, multi layered epithelium over the whole graft; in some points at the wound margins, it formed buds extending toward the underlying stroma, conceivably representing proliferative cell compartments. The graft tissue appeared thinner but better organized than that of the other samples (Groups 1 and 2) and was often virtually indistinguishable from the adjacent tissues at the wound bed.

These results confirmed that both *in situ* bioprinted grafts can improve wound healing, fill the wound bed, and facilitate re-epithelization. These phenomena were particularly enhanced in the fibroblast-seeded CELLINK Fibrin hydrogel group, which showed superior performance in efficiently closing the wound and promoting the regrowth of the surface epithelium, thereby restoring a barrier to the external environment. Of note, no histological signs of adverse side effects induced by the graft were observed in the tissues surrounding the wound.

These findings confirmed that the bioink composed of CELLINK Fibrin hydrogel and human dermal fibroblasts is a suitable substrate for 3D bioprinting in wound care. Next, we applied it to test a new wound care model comprising *in situ* 3D grafting and NIR laser treatment.

3.3. Effectiveness of the new wound care protocol on graft integration and wound healing

The described protocol for wound management, based on *in situ* 3D bioprinting of the fibroblast-seeded (nHDF) CELLINK Fibrin hydrogel, followed by NIR laser treatment to promote graft integration and stimulate healing, was assessed. For these tests, the leeches (n=16) were subjected to standard tegument tissue wounds, as described in **Section 2.2**, and then divided into four groups:

(i) Untreated animals (n=4) with no *in situ* 3D bioprinting and NIR laser treatment, taken as negative controls.

(ii) Animals that received a graft of CELLINK Fibrin-nHDF produced through *in situ* 3D bioprinting (n=4; CELLINK Fibrin-nHDF).

(iii) Animals that received NIR laser treatment (n=4).

(iv) Animals that received a graft of CELLINK Fibrin-nHDF followed by NIR laser treatment (n=4; CELLINK Fibrin-nHDF+NIR laser).

Six hours after the last laser treatment, the animals were processed for histological sampling and analysis, as described in **Sections 2.11 and 2.12**.

3.3.1. Morphological analysis using hematoxylin and eosin staining

The morphological features at the wound site were first analyzed using the H&E-stained slides. The sections from the untreated controls showed features similar to those of the same controls of the previous experiment: the surface epithelium was extremely thin, and the underlying connective tissue formed a loose meshwork (Figure 3A). The sections from the leeches grafted with CELLINK Fibrin-nHDF showed a thicker, multi layered epithelium over a thin connective tissue containing newly formed blood capillaries (Figure 3B). The sections from the leeches treated with NIR laser alone showed a thin,

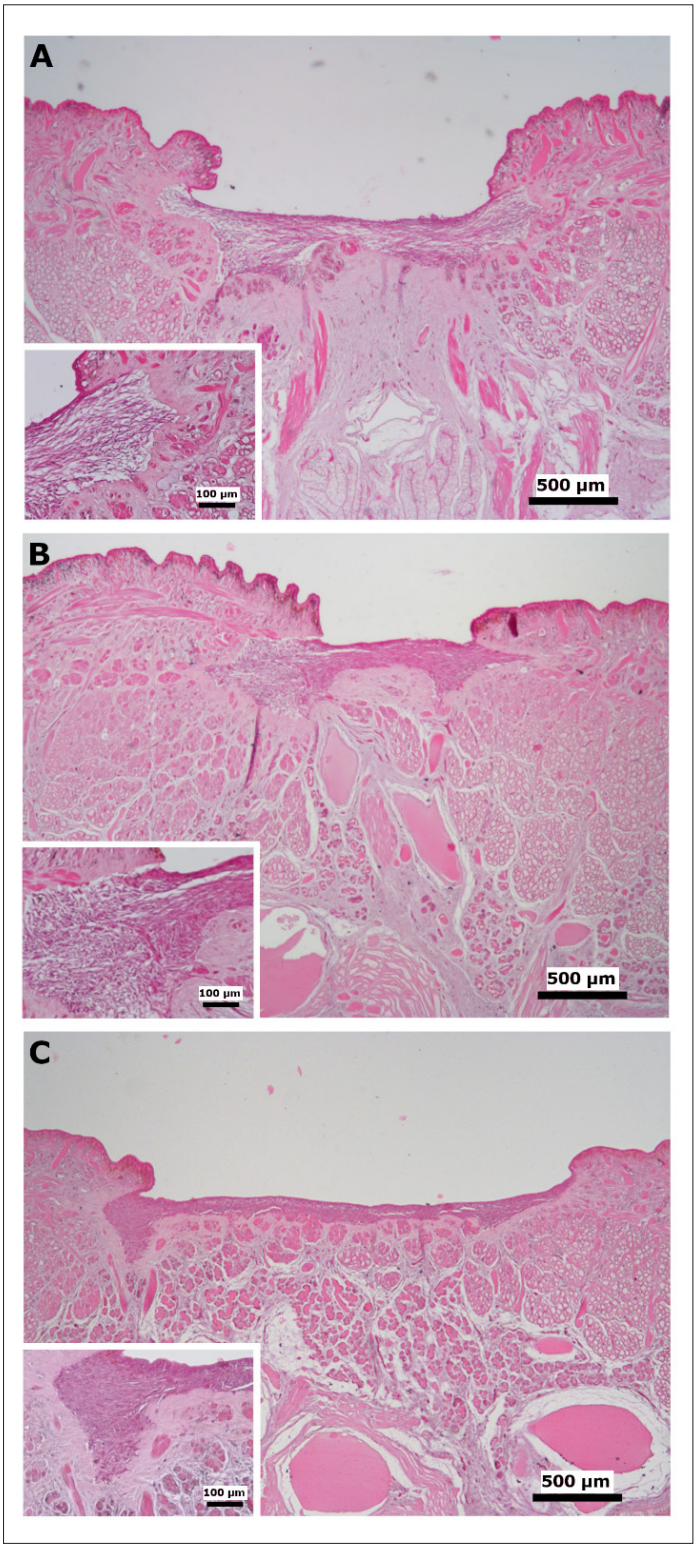

Figure 2. Validation of *in situ* 3D bioprinting procedure for leech wound healing using alginate and gelatin (SA-GEL) hydrogel and CELLINK Fibrin hydrogel containing normal human dermal fibroblasts. Comparative analysis of the different experimental conditions using hematoxylin and eosin staining. (A) Untreated control leech, showing early healing. (B) Leech grafted with SA-GEL hydrogel, showing a denser sub-epithelial supporting matrix. (C) Leech grafted with CELLINK Fibrin hydrogel containing human dermal fibroblasts, showing improved re-epithelization of the wound. Scale bars: 500 µm, insets:100 µm; magnifications: 4×, insets: 20×.

sometimes incomplete epithelium that, at the wound margins, formed buds of proliferating cells growing into the underlying stroma; it lay over a hyperplastic connective tissue featuring granulation tissue, rich in dilated blood capillaries (Figure 3C). The sections from the leeches grafted with CELLINK Fibrin-nHDF+NIR laser showed the most advanced wound healing, with a thick epithelium continuous with the perilesional tissue, overlaying connective tissue with a normal appearance similar to that beyond the wound margins (Figure 3D).

3.3.2. Analysis of collagen fibers

Collagens play a crucial role in the healing process by providing a scaffold that supports tissue regeneration, facilitates cell migration, and contributes to the mechanical strength and integrity of the newly formed ECM.[33] On the other hand, excessive formation of collagen fibers can lead to hypertrophic scars and fibrosis. Therefore, the network of collagen fibers at the wound site was studied using Picrosirius red staining. In untreated controls, the connective tissue surrounding the wound exhibited a dense network of collagen fibers, which thinned to an extremely thin layer at the wound bed (Figure 4A). In the sections from the CELLINK Fibrin-nHDF group, collagen fibers formed a well-defined, dense layer under the thickened surface epithelium (Figure 4B). In the NIR laser treatment group, collagen fibers also formed a well-defined layer under the epithelial buds and were abundant, albeit loosely arranged, in the granulation tissue at the wound area (Figure 4C). In the sections from the CELLINK Fibrin-nHDF + NIR laser group, a continuous layer of loosely woven collagen fibers was present under the newly formed epithelium, extending

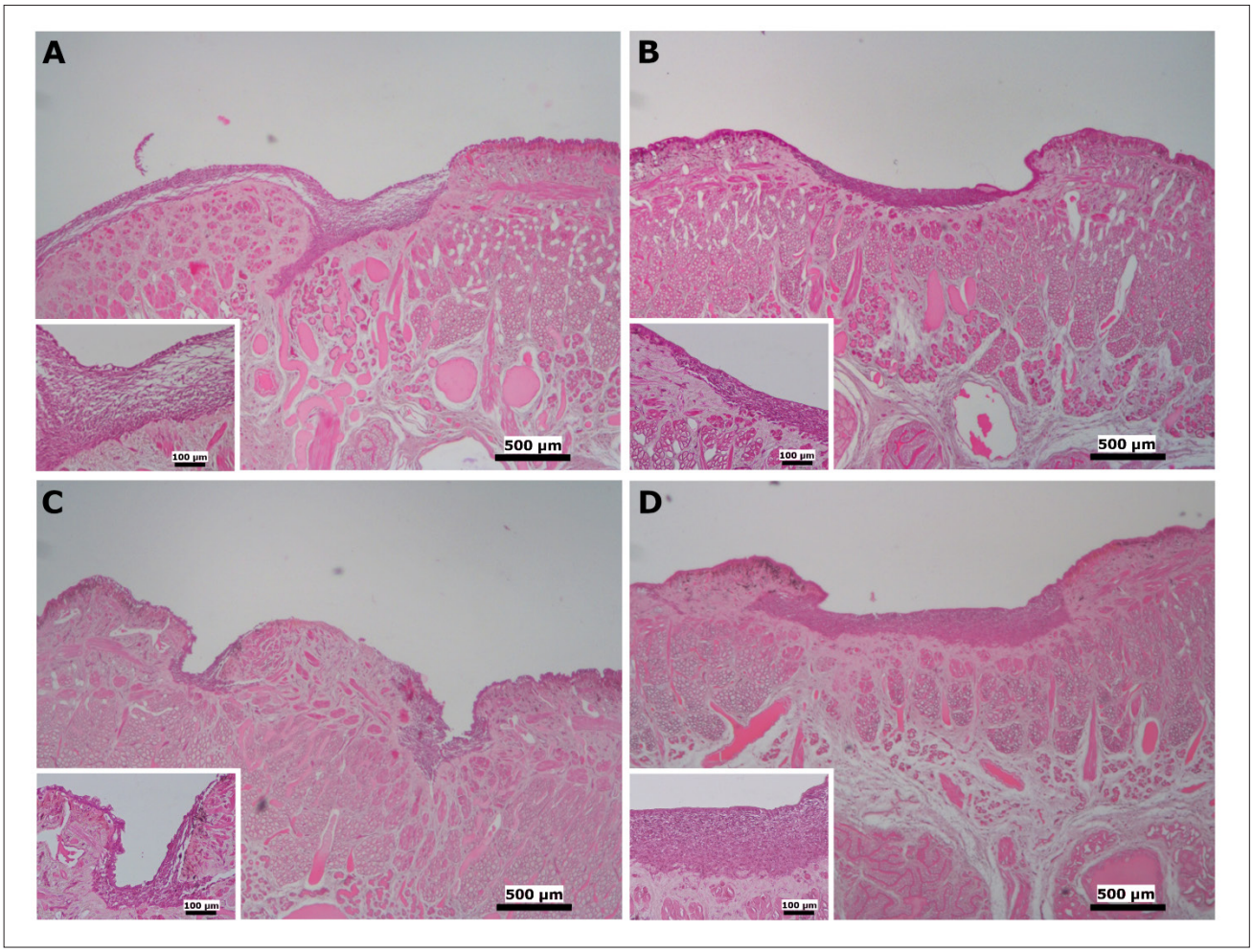

Figure 3. Effect of *in situ* 3D bioprinting procedure and near-infrared (NIR) laser treatment on leech wound healing. Comparative analysis of the different experimental conditions using hematoxylin and eosin staining. (A) Untreated control leech, showing early healing. (B) Leech grafted with CELLINK Fibrin-normal human dermal fibroblasts (nHDF), showing improved re-epithelialization of the wound. (C) Leech treated with NIR laser alone, showing marginal epithelial regrowth and neo-angiogenesis. (D) Leech grafted with CELLINK Fibrin-nHDF + NIR laser, showing markedly thicker surface epithelium and nearly normal underlying connective tissue. Scale bars: 500 µm, insets:100 µm; magnifications: 4×, insets: 20×.

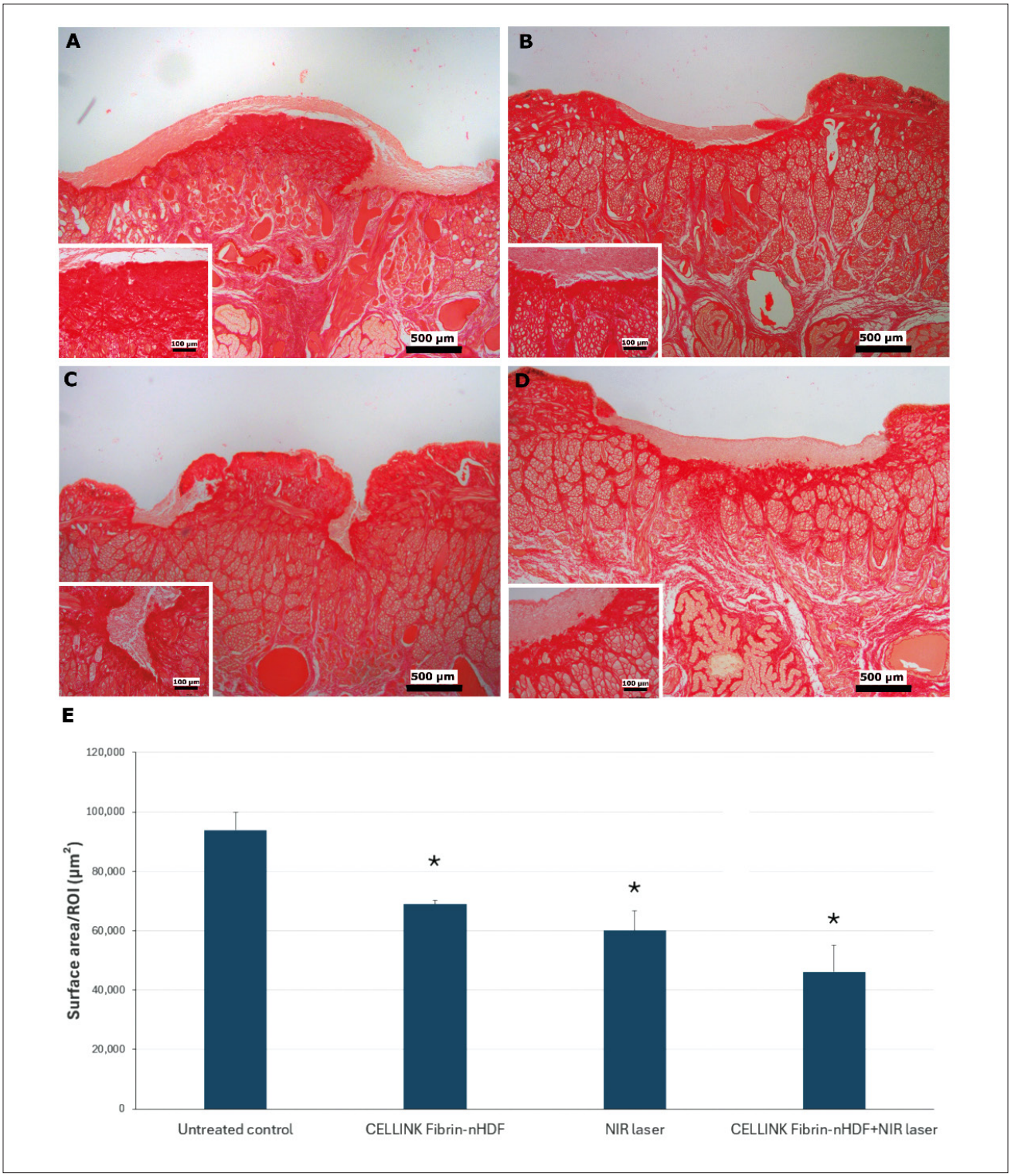

Figure 4. Effect of *in situ* 3D bioprinting procedure and near-infrared (NIR) laser treatment on leech wound healing. Comparative analysis of the Picrosirius red- stained collagen fiber network across experimental groups. (A) Untreated control. (B) Leech grafted with CELLINK Fibrin-normal human dermal fibroblasts (nHDF). (C) Leech treated with NIR laser radiation alone. (D) Leech grafted with CELLINK Fibrin-nHDF + NIR laser. See the text for details. Scale bars: 500 µm, insets:100 µm; magnifications: 4×, insets: 20×. (E) Morphometric analysis of the amount of collagen fibers across experimental groups. Notes: *$p < 0.05$, determined by one-way ANOVA followed by multiple comparison tests. All comparisons are made relative to the untreated control group. Abbreviation: ROI: Region of interest.

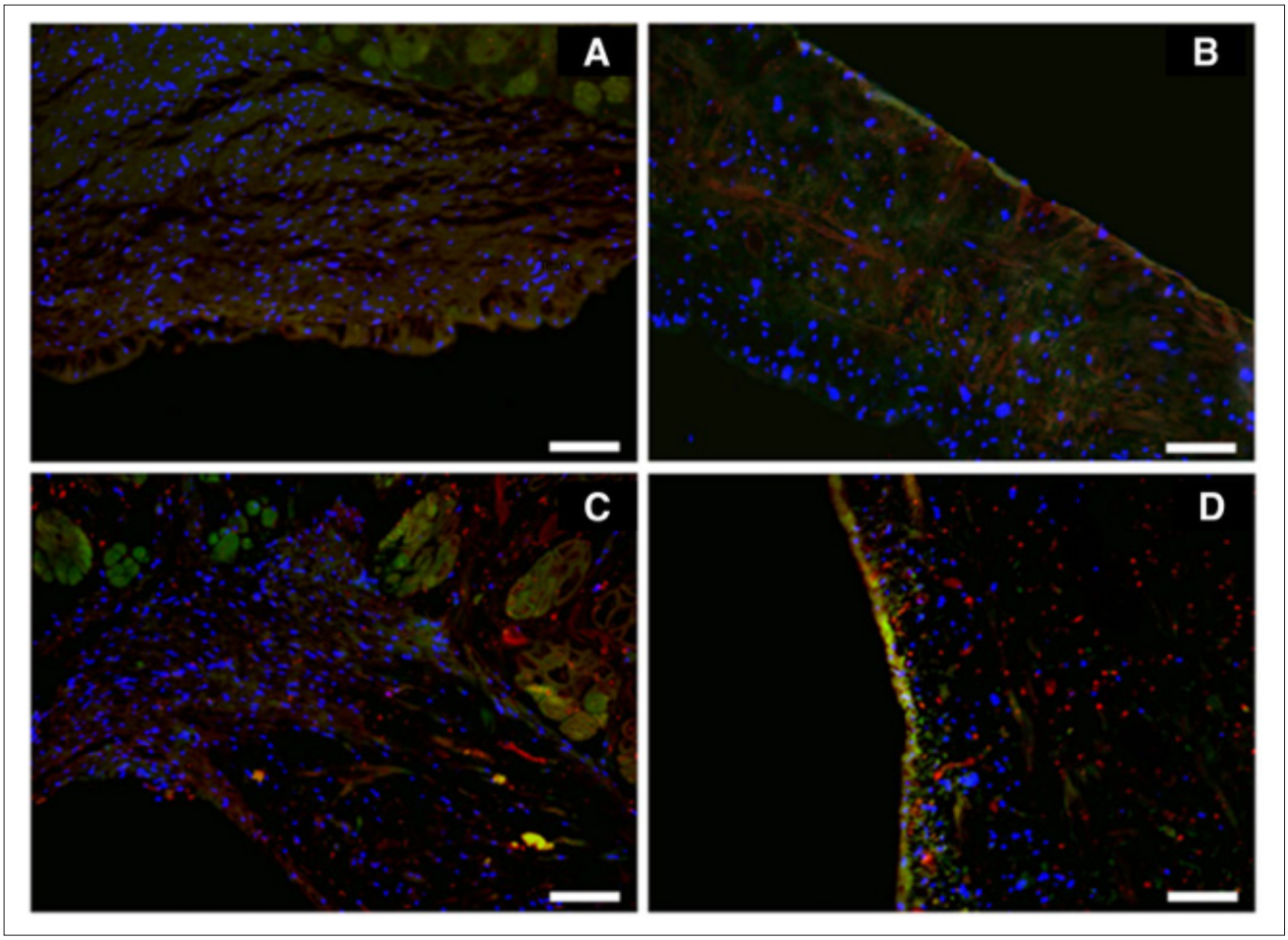

Figure 5. Effect of *in situ* 3D bioprinting procedure and near-infrared (NIR) laser treatment on leech wound healing. Immunofluorescent co-localization of HSP47 (red) and α-SMA (green) fibroblast activation markers across experimental groups. Cell nuclei are counterstained with DAPI (blue). (A) Untreated control. (B) Leech grafted with CELLINK Fibrin-normal human dermal fibroblasts (nHDF). (C) Leech treated with NIR laser radiation alone. (D) Leech grafted with CELLINK Fibrin-nHDF + NIR laser treatment shows well-detectable expression of HSP47 and α-SMA. Scale bars: 50 μm, magnifications: 20×. Abbreviations: α-SMA: Alpha smooth muscle actin; DAPI: 4´,6-diamidino-2-phenylindole; HSP47: Heat shock protein 47.

into the stroma of the deeper muscle tissues (Figure 4D). The collagen meshwork at the wound margins appeared continuous with that of the wound area, suggesting tissue integration. The absence of a dense collagen layer in this group suggests that this treatment could have reduced the local inflammatory response, potentially limiting fibrosis. The morphometric analysis of Picrosirius red-stained collagen fiber content in the wound area confirmed these observations (Figure 4E).

3.3.3. Analysis of fibroblast markers

Immunofluorescence analysis was performed to evaluate the expression of key fibroblast markers. HSP47, a collagen-specific chaperonin essential for proper folding, assembly, and secretion of collagen during ECM production and tissue repair,[34] is assumed to be a pan-fibroblast marker. Alpha-SMA is believed to be a marker for the fibroblast-to-myofibroblast switch, which is crucial for wound contraction and tissue remodeling, as well as for hypertrophic scarring and fibrosis.[35] The results showed that the samples from the negative controls (Figure 5A), the CELLINK Fibrin-nHDF group (Figure 5B), and the NIR laser treatment group (Figure 5C) did not exhibit significant fluorescence, except for a slight HSP 47- positive signal in the NIR laser treatment group, indicating that the cell expression of HSP47 (red) and α-SMA (green) was negligible in these groups. In contrast, the samples from the CELLINK Fibrin-nHDF + NIR laser group (Figure 5D) showed a substantial cell expression of HSP 47 and α-SMA. This finding suggests that in this group, fibroblast recruitment and activation occur to promote healing, a result in agreement with the data from conventional histology and collagen histochemistry.

4. Discussion

The advantages of *in situ* 3D bioprinting, compared to *in vitro* 3D bioprinting and subsequent grafting of the tissue construct into an organism, have been widely highlighted in recent literature.[36,37] It is well known that the culture and maturation of a biofabricated tissue are regulated by numerous biochemical and biophysical factors that can hardly be reproduced *in vitro*, especially considering the unavoidable time gap between printing and grafting. The physiological environment is dynamic, continuously evolving to maintain or restore homeostasis, which challenges attempts to mimic it accurately *in vitro*.[38] Furthermore, *in vitro* culture of biofabricated tissues requires dedicated facilities, prolonged timeframes, higher costs, and repeated handling of samples, all of which increase the risk of microbial contamination, loss of structural integrity, and compromised geometric fit with the recipient site.[39,40] Therefore, the *in situ* bioprinting technique was chosen for the development of the wound care model in this study.

The *in situ* 3D bioprinting procedure in the leech model was complex. The leech is an annelid; it has a wavy integument, and even under anesthesia, slight body movements can result in lengthening or shortening of the body, leading to deformation of the wound bed. Therefore, the *in situ* 3D bioprinting procedure used in the present study required careful preparation and a series of validation tests.

In preparation for the experiments with the animal model, the 3D bioprinting protocol software was successfully validated through 2D printing tests—producing differently shaped monolayers—and 3D printing tests, creating multilayered structures (four layers) of different shapes and sizes to simulate the grafts intended for the *in vivo* experiments. Following these preliminary tests, the *in situ* 3D bioprinting procedure was further validated using a leech phantom. This test showed that the developed protocol allowed a graft to be successfully printed within the wound model created on the phantom.

Before evaluating the effectiveness of the proposed wound care strategy (3D bioprinting followed by NIR laser irradiation), the *in situ* 3D bioprinting procedure was additionally tested on the animal model. Initially, a SA-GEL hydrogel crosslinked with $CaCl_2$ was used as the bioink. Then, a $CaCl_2$-crosslinked CELLINK Fibrin hydrogel mixed with human dermal fibroblasts was tested. Both tests confirmed the feasibility of the *in situ* 3D bioprinting procedure without adverse effects on the animals. In particular, the human dermal fibroblasts embedded in the CELLINK Fibrin hydrogel did not elicit a rejection response, as leeches have a rudimentary immune system. They lack a complex adaptive component and rely primarily on innate immunity, which is incapable of developing long-term immunological memory against specific antigens. Furthermore, as blood-sucking parasites, leeches have evolved tolerance to blood components from different species and produce anticoagulant substances in their saliva.

The fibrinogen-based hydrogel was chosen as a suitable environment for human dermal fibroblasts because previous experiments showed its superior ability to preserve cell viability[26] and function compared to SA-GEL.[21] Specifically, in the study by Cavallo *et al.*[26], a cell viability of 94 ± 4% was demonstrated using L929 fibroblasts embedded in a fibrinogen- and alginate-based hydrogel, with no cytotoxic effect from the biomaterial ink observed.

Histological analyses of tissue samples collected four days after 3D bioprinting demonstrated that: (i) graft deposition procedure within the wound was successful using both hydrogels; (ii) the SA-GEL-based graft improved wound healing compared to untreated wounds; and (iii) the CELLINK Fibrin hydrogel containing human dermal fibroblasts induced more effective activation of healing mechanisms compared to both untreated and SA-GEL-grafted wounds (Figure 2). On this basis, the CELLINK Fibrin hydrogel was selected for further *in vivo* experiments to validate the proposed wound care protocol.

In some protocols, the CELLINK Fibrin hydrogel is added with thrombin to convert fibrinogen into fibrin. However, the construct should then be washed thoroughly, as thrombin residues can affect cell viability.[26] Because *in situ* bioprinting only allows partial washing (on the exposed side), $CaCl_2$ crosslinking was preferred. Furthermore, a previous study showed that converting fibrinogen to fibrin did not significantly enhance cell viability and function preservation.[21]

As reported, the major advantage of *in situ* bioprinting over *in vitro* bio fabrication is that the graft is directly placed in its recipient area, within a physiological environment that provides the necessary biochemical and biophysical signals to support tissue maturation. However, this environment is highly dynamic and responds to wound damage and grafting. In response to injury, a complex repair process rapidly takes place through several phases, each partially overlapping and tightly regulated qualitatively, quantitatively, and temporally. Briefly, the immediate hemostatic phase is followed by the inflammatory phase, which prevents infection and induces stromal activation through the production of pro-inflammatory factors by innate and immune cells. The proliferative phase then occurs, characterized by neoangiogenesis, granulation

tissue formation, and re-epithelialization, involving fibroblasts, endothelial cells, and surface epithelial cells. Finally, during the remodeling phase, fibroblasts remodel the ECM of the newly formed tissue to improve its structure and function. Endothelial cells and the stem cell compartment of the surface epithelium are responsible for neoangiogenesis and re-epithelialization, respectively, whereas fibroblasts are involved in all phases of healing by orchestrating the process through continuous cross-talk with other cell populations. The transition between healing phases is primarily regulated by apoptosis: cell populations that have completed their function in the damaged area undergo programmed cell death and are replaced by newly recruited cell populations required for the next phase.[3,41]

When the graft is bioprinted into the wound bed, it is surrounded by tissues undergoing an inflammatory reaction, which can be exacerbated by the presence of engrafted exogenous material. Acute inflammation is required to initiate repair mechanisms and can facilitate graft maturation by promoting cell migration, neoangiogenesis, and ECM production. However, excessive or persistent inflammation can lead to abnormal stromal cell activation, excessive capillary formation, and ECM deposition, potentially resulting in the formation of fibrous tissue encapsulating the graft[42] and hindering its integration. In summary, an overly intense or prolonged inflammatory response jeopardizes repair mechanisms and compromises the interaction between the graft and the surrounding tissues. Therefore, several strategies have been proposed to control inflammation upon grafting.[42]

Based on our previous research on the anti-inflammatory properties of NIR laser radiation,[29] we hypothesized that NIR laser treatment could be an effective and easy-to-implement strategy to modulate inflammation at the graft site. Accordingly, the proposed wound care protocol, designed to improve the healing of wounds with loss of substance (in the leech model, loss of tegumental tissue), consists of two treatments: (i) *in situ* 3D bioprinting of a graft composed of CELLINK Fibrin hydrogel containing human dermal fibroblasts directly into the wound bed; (ii) additional treatment of the wound and surrounding tissues via irradiation with an NIR laser source. The working hypotheses were twofold: (i) the *in situ* bioprinting of the graft was hypothesized to promote tissue regeneration by protecting the wound from microorganisms and external factors, thus decreasing the risk of contamination. Moreover, by replacing lost tissue with a protein network and a nanofibrillated cellulose matrix containing dermal fibroblasts, the graft was expected to support cell repopulation and tissue remodeling. (ii) The adjunctive NIR laser treatment was hypothesized to promote graft integration with surrounding tissues, accelerate healing, and prevent fibrosis through its dual effects—inhibitory effects on inflammatory response and stimulatory effects on cell energy metabolism, production, and assembly of ECM molecules.[27,29]

To test the above hypotheses, four groups of differently treated animals were compared: (i) untreated controls, (ii) *in situ* 3D bioprinting only, (iii) NIR laser irradiation only, and (iv) the combined treatment. As hypothesized, the *in situ* bioprinted grafts significantly improved wound healing. Untreated controls showed a particularly thin surface epithelium and an underlying connective tissue that appeared as a loose meshwork containing few cells, clearly distinct from the surrounding tissues. In contrast, leeches grafted with the fibrinogen hydrogel containing human dermal fibroblasts showed a thicker, multilayered epithelium throughout the graft, accompanied by the formation of proliferative cellular compartments.

For this result, a crucial aspect is the choice of biomaterial ink and its degree of degradation, which must support proper wound filling and allow the gradual regeneration of the animal's native tissue. In this regard, the degradation of fibrinogen- and alginate-based hydrogels was studied in detail by Cavallo *et al.*[26] In their study, a mass loss of approximately 20% was observed in bioprinted samples during the first week of incubation (Figure S11). The mass remained nearly constant over the following three weeks, followed by an increase in degradation during the fifth week. In our application, this gradual degradation of the hydrogel ensured appropriate wound filling on the leech's back and provided protection from microorganisms and external factors, thus reducing the risk of contamination. Furthermore, by replacing the lost tissue with a network of proteins and a nanofibrillated cellulose matrix containing dermal fibroblasts, the graft, as hypothesized, promoted cell repopulation and subsequent tissue remodeling.

Conventional histological analysis, quantitative histochemical assay of the collagen fiber network, and immunofluorescence detection of activated fibroblasts in healing tissues concur to indicate that leeches that received the combined treatment—*in situ* bioprinting followed by laser treatment—showed favorable results in terms of the rate and quality of graft integration and tissue regeneration. In particular, re-epithelialization was nearly complete, and the underlying stromal tissue appeared well-structured, free from signs of fibrosis, and tightly connected to the surrounding tissues (Figure 4D).

In untreated animals and those receiving the *in situ* 3D-bioprinted graft, histochemical and morphometric analyses of collagen fibers revealed a thick fibrotic network extending into the adjacent tissues (Figure 4A and 4B). Fibrotic tissue is generally an expression of excessive

and/or prolonged inflammation. In the animals treated with laser radiation alone, fibrosis was reduced; however, a hyperplastic mass of granulation tissue —apparently impeding complete re-epithelization—was often observed (Figure 4C). These findings confirm the synergism between the *in situ* bioprinted grafts and NIR laser irradiation to achieve optimal healing effects. They also support previous observations that NIR laser treatment can effectively limit fibrosis, potentially through its modulatory effects on inflammation and on ECM protein deposition, including collagen.

As mentioned above, fibroblasts play a key role in wound healing. Once activated, they regulate the activity of the other cell populations that participate in the healing process. Furthermore, upon differentiation into contractile myofibroblasts, they induce wound contraction and ECM remodeling.[3,31] The findings on HSP47 and α-SMA expression, analyzed by immunofluorescence microscopy, suggest that this activation occurred only in animals receiving both *in situ* bioprinting and laser treatment, in which these markers were clearly detected, indicating a more advanced stage of healing. In the other experimental groups, no significant expression of these markers was detected, suggesting that fibroblast recruitment was still at an early stage or potentially impaired.

In situ 3D bioprinting is an emerging technology, whereas NIR laser therapy has been applied to promote the healing of acute and chronic lesions for several years. The pro-regenerative effects of NIR laser radiation have been widely reported in the literature, with extensive information spanning from the molecular to the clinical level.[3,43,44] However, to our knowledge, this is the first study to apply NIR laser irradiation to support the engraftment of a biofabricated tissue construct directly within the wound bed.

The main limitations of this study include: (i) the small number of animals per experimental group, which requires caution when generalizing the results; and (ii) the use of a small invertebrate animal model, in which the wound area and the volume of dead space are proportionate to body size. Nevertheless, the leech model has been recognized as a valuable tool for studying the regeneration of human skin,[16] and has the advantage of being particularly suitable for experiments conducted in extreme environments, such as space platforms.

In relatively small wounds, such as those adopted in this study, re-epithelialization occurs spontaneously from the wound margins, especially when aided by a graft that simulates dermal functions—particularly fibroblast activity, which promotes keratinocyte proliferation and migration through cytokine release.[2] In large wounds, the current model could be extended by printing an additional superficial layer containing keratinocytes, thereby mimicking the epidermis to further accelerate wound closure and restoration of the skin barrier. This is a key aspect in view of future clinical applications and will be investigated in future research.

Despite the promising results obtained with the proposed wound management protocol, clinical translation remains highly challenging. The main issues include: (i) the development of 3D bioprinters suitable for the clinical setting, ideally at the patient's bedside; and (ii) the fabrication of grafts large enough to cover extended wound areas or substantial tissue loss. Large wounds pose critical challenges related to re-epithelialization and vascularization. Vascularization is essential for graft survival, as passive transport mechanisms, such as diffusion, become insufficient once the graft exceeds a certain size. Re-epithelialization and vascularization will therefore be central topics in our future research aimed at improving the proposed model. Another challenge is that producing grafts of clinically relevant dimensions requires substantially more cells, making cell supply a significant bottleneck.

In summary, the scaling challenges for human applications include developing efficient cell-expansion protocols and strategies for printing complex grafts incorporating two or more distinct cell populations, such as fibroblasts, keratinocytes, and endothelial cells. Endothelial cells are essential for supporting the formation of a capillary network, which is crucial in larger constructs to ensure adequate nutrients and oxygen delivery.

Implementing this approach in extreme environments, particularly aboard space platforms, poses additional challenges, including: (i) the adaptation of equipment for use in space, i.e., the development of hardware (3D bioprinter and laser source) that meets safety and operational criteria in space; (ii) strict control over the 3D bioprinting process to ensure product quality and prevent biological contamination within the spacecraft environment; and (iii) the limited current knowledge of how space environment affects 3D-bioprinted constructs. To advance this knowledge, it may be useful to study the behavior of long-term (≥ 3 weeks) tissue-construct cultures under simulated microgravity. While microgravity favors the formation of cellular aggregates, the combined effects of microgravity and space radiation can profoundly alter cellular functions, including proliferation, differentiation, apoptosis, ECM production, and cell-to-cell cross-talk, potentially compromising the survival and proper maturation of the constructs. Therefore, detailed studies

are needed to assess the maturation of 3D-bioprinted constructs and the fate of the embedded cells.

5. Conclusion

The wound treatment protocol proposed in this study—combining *in situ* 3D bioprinting with NIR laser treatment—has demonstrated effectiveness in promoting the engraftment of 3D-printed tissue constructs and in activating intrinsic wound healing mechanisms. These findings may pave the way for innovative strategies for managing severe wounds and burns, for which current treatments are often complex and expensive, healing times are prolonged, and undesirable sequelae such as fibrosis are common. The implementation of new wound-healing therapies is particularly relevant in extreme environments—such as space platforms, submarines, and Arctic and Antarctic bases—or under extreme conditions, including military operations, terrorist strikes, and natural disasters, where the management of severe injuries becomes particularly challenging.

Acknowledgments

None.

Funding

This research was funded by the Italian Space Agency (ASI) under the projects GROWS (C-ASI No. 2021-16-U.0), WEAR ME! (ASI No. 2023-3-U.0), and SATURNO (ASI No. 2024-12-U.0). Support to this study was also provided by the European Space Agency (ESA) through the selection of the GROWS project and funding of the WHISPER project (No. 4000130928/20/NL/PG/pt). Additional support was provided by the European Union (ERC, EPEIUS, Grant Agreement No. 101125466). This study was also partially supported by the Ricerca Corrente funding from the Italian Ministry of Health to IRCCS Policlinico San Donato.

Conflict of interest

The authors declare they have no competing interests.

Author contributions

Conceptualization: Monica Monici, Michele Conti
Formal analysis: Francesca Cialdai, Chiara Risaliti, Lorenzo Notari, Daniele Bani
Funding acquisition: Monica Monici, Michele Conti
Investigation: Giada Loi, Mariagrazia Zaccara, Francesca Cialdai, Chiara Risaliti, Lorenzo Notari, Glenda Liggieri
Methodology: Monica Monici, Michele Conti, Daniele Bani
Supervision: Monica Monici, Michele Conti, Daniele Bani
Writing–original draft: Giada Loi, Mariagrazia Zaccara, Francesca Cialdai, Chiara Risaliti, Lorenzo Notari, Glenda Liggieri
Writing–review & editing: Monica Monici, Michele Conti, Daniele Bani

Ethics approval and consent to participate

Since leeches are invertebrates, Animal Ethics Committee approval is not required for their use in research. However, in this study, the animals were treated in accordance with strict ethical principles to avoid suffering, and all treatments were performed under anesthesia.

Consent for publication

Not applicable.

Availability of data

The data that support the findings of this study are available from the corresponding author upon reasonable request.

References

1. Sorg H, Sorg CGG. Skin Wound Healing: of Players, patterns, and processes. *Eur Surg Res.* 2023;64(2):141-157. doi: 10.1159/000528271
2. Peña OA, Martin P. Cellular and molecular mechanisms of skin wound healing. *Nat Rev Mol Cell Biol.* 2024;25(8):599-616. doi: 10.1038/s41580-024-00715-1
3. Cialdai F, Risaliti C, Monici M. Role of fibroblasts in wound healing and tissue remodeling on Earth and in space. *Front Bioeng Biotechnol.* 2022;10:958381. doi: 10.3389/fbioe.2022.958381
4. Darby IA, Hewitson TD. Fibroblast differentiation in wound healing and fibrosis. *Int Rev Cytol.* 2007;257:143-79. doi: 10.1016/S0074-7696(07)57004-X
5. Martin P, Pardo-Pastor C, Jenkins RG, Rosenblatt J. Imperfect wound healing sets the stage for chronic diseases. *Science*. 2024;386(6726):eadp2974. doi: 10.1126/science.adp2974
6. Sen CK. Human Wound and Its Burden: Updated 2022 Compendium of Estimates. *Adv Wound Care (New Rochelle).* 2023;12(12):657-670. doi: 10.1089/wound.2023.0150
7. Avishai E, Yeghiazaryan K, Golubnitschaja O. Impaired wound healing: facts and hypotheses for multi-professional considerations in predictive, preventive and personalised medicine. *EPMA J.* 2017;8(1):23-33. doi: 10.1007/s13167-017-0081-y

8. Hongying Z, Chunmei H, Lijuan C, *et al*. The current status and influencing factors of quality of life of chronic wound patients based on Wound-QoL scale: a cross-sectional study. *Medicine (Baltimore)*. 2025;104(27):e42961. doi: 10.1097/MD.0000000000042961

9. Harding K, Gray D, Timmons J, Hurd T. Evolution or revolution? Adapting to complexity in wound management. Int Wound J. 2007;4(Suppl 2):1-12. doi: 10.1111/j.1742-481X.2007.00329.x

10. Radzikowska-Büchner E, Łopuszyńska I, Flieger W, Tobiasz M, Maciejewski R, Flieger J. An overview of recent developments in the management of burn injuries. *Int J Mol Sci*. 2023;24(22):16357. doi: 10.3390/ijms242216357

11. Kirkpatrick AW, Ball CG, Campbell M, Williams DR, Parazynski SE, Mattox KL, Broderick TJ. Severe traumatic injury during long duration spaceflight: Light years beyond ATLS. *J Trauma Manag Outcomes*. 2009;3:4. doi: 10.1186/1752-2897-3-4

12. Balukoff NC, Houk G, Gonzalez T, *et al*. Out of this World: wound healing on earth and in space. *J Invest Dermatol*. 2025;145(8):1879-1895. doi:10.1016/j.jid.2024.12.024

13. Pantalone D. Surgery in the next space missions. *Life*. 2023;13(7):1477. doi: 10.3390/life13071477

14. Cubo-Mateo N, Gelinsky M. Wound and skin healing in space: the 3D Bioprinting Perspective. *Front Bioeng Biotechnol*. 2021;9:720217. doi: 10.3389/fbioe.2021.720217

15. Klarmann GJ, Rogers AJ, Gilchrist KH, Ho VB. 3D bioprinting meniscus tissue onboard the International Space Station. *Life Sci Space Res (Amst)*. 2024;43:82-91. doi: 10.1016/j.lssr.2024.09.004

16. Tettamanti G, Grimaldi A, Congiu T, Perletti G, Raspanti M, Valvassori R, de Eguileor M. Collagen reorganization in leech wound healing. *Biol Cell*. 2005;97(7):557-68. doi: 10.1042/BC20040085

17. Grimaldi A, Banfi S, Bianchi C, *et al*. The leech: a novel invertebrate model for studying muscle regeneration and diseases. *Curr Pharm Des*. 2010;16(8):968-77. doi: 10.2174/138161210790883417

18. Cialdai F, Colciago A, Pantalone D, *et al*. Effect of unloading condition on the healing process and effectiveness of platelet rich plasma as a countermeasure: study on *In vivo* and *In vitro* wound healing models. *Int J Mol Sci*. 2020;21(2):407. doi: 10.3390/ijms21020407

19. Baranzini N, Pulze L, Tettamanti G, Acquati F, Grimaldi A. *Hv*RNASET2 regulate connective tissue and collagen I remodeling during wound healing process. *Front Physiol*. 2021;12:632506. doi: 10.3389/fphys.2021.632506

20. Lotz RG, Baum P, Bowman GH, Klein KD, von Lohr R, Schrotter L. Test of a life support system with Hirudo medicinalis in a sounding rocket. *Life Sci. Space Res*. 1972;10:133–143.

21. Ronzoni FL, Aliberti F, Scocozza F, *et al*. Myoblast 3D bioprinting to burst *in vitro* skeletal muscle differentiation. *J Tissue Eng Regen Med*. 202216(5):484–495. doi: 10.1002/term.3293

22. Delgrosso E, Scocozza F, Cansolino L, *et al*. 3D bioprinted osteosarcoma model for experimental boron neutron capture therapy (BNCT) applications: Preliminary assessment. *J Biomed Mater Res B Appl Biomater*. 2023;111(8): 1571-1580. doi: 10.1002/jbm.b.35255

23. Loi G, Scocozza F, Aliberti F, *et al*. 3D Co-Printing and Substrate Geometry Influence the Differentiation of C2C12 Skeletal Myoblasts. *Gels*. 2023; 9(7):595. doi: 10.3390/gels9070595

24. Loi G, Scocozza F, Benedetti L, *et al*. Design, development, and benchmarking of a bioreactor integrated with 3D bioprinting: application to skeletal muscle regeneration. *Bioprinting*. 2024;42:e00352. doi: 10.1016/j.bprint.2024.e00352

25. Fantini V, Bordoni M, Scocozza F, *et al*. Bioink composition and printing parameters for 3D modeling neural tissue. *Cells*. 2019;8(8):830. doi: 10.3390/cells8080830

26. Cavallo A, Al Kayal T, Mero A, *et al*. Fibrinogen-Based Bioink for application in skin equivalent 3D Bioprinting. *J Funct Biomater*. 2023;14(9):459. doi: 10.3390/jfb14090459

27. Monici M, Basile V, Cialdai F, Romano G, Fusi F, Conti A. Irradiation by pulsed Nd: YAG laser induces the production of extracellular matrix molecules by cells of the connective tissues: a tool for tissue repair. Biophotonics: Photonic solutions for better health care. Edited by Popp Jürgen, Drexler Wolfgang, Tuchin Valery V, Matthews Dennis L. Proceedings of the SPIE. 2008;6991:10.

28. Monici M, Cialdai F, Romano G, Fusi F, Egli M, Pezzatini S. An *in vitro* study on tissue repair: impact of unloading on cells involved in the remodelling phase. *Microgravity Sci Technol*. 2011;23:391–401. doi:10.1007/s12217-011-9259-4

29. Genah S, Cialdai F, Ciccone V, Sereni E, Morbidelli L, Monici M. Effect of NIR laser therapy by MLS-MIS source on fibroblast activation by inflammatory cytokines in relation to wound healing. *Biomedicines*. 2021;9(3):307. doi: 10.3390/biomedicines9030307

30. Barrientos S, Stojadinovic O, Golinko MS, Brem H, Tomic-Canic M. Growth factors and cytokines in wound healing. Wound Repair Regen. 2008;16(5):585-601. doi: 10.1111/j.1524-475X.2008.00410.x

31. Moretti L, Stalfort J, Barker TH, Abebayehu D. The interplay of fibroblasts, the extracellular matrix, and inflammation in scar formation. *J Biol Chem.* 2022;298(2):101530. doi: 10.1016/j.jbc.2021.101530

32. Younesi FS, Miller AE, Barker TH, Rossi FMV, Hinz B. Fibroblast and myofibroblast activation in normal tissue repair and fibrosis. *Nat Rev Mol Cell Biol.* 2024;25(8):617-638. doi: 10.1038/s41580-024-00716-0

33. Gardeazabal L, Izeta A. Elastin and collagen fibres in cutaneous wound healing. *Exp Dermatol.* 2024;33(3):e15052. doi: 10.1111/exd.15052

34. Ito S, Nagata K. Roles of the endoplasmic reticulum-resident, collagen-specific molecular chaperone Hsp47 in vertebrate cells and human disease. *J Biol Chem.* 2019;294(6):2133-2141. doi: 10.1074/jbc.TM118.002812

35. McAndrews KM, Miyake T, Ehsanipour EA, *et al*. Dermal αSMA+ myofibroblasts orchestrate skin wound repair via β1 integrin and independent of type I collagen production. *EMBO J*. 2022;41(7):e109470. doi: 10.15252/embj.2021109470

36. Singh S, Choudhury D, Yu F, Mironov V, Naing MW. *In situ* bioprinting – Bioprinting from benchside to bedside? *Acta Biomaterialia.* 2020;101(2020):14–25 doi: 10.1016/j.actbio. 2019.08.045

37. Hu C, Wang C, Bian S, *et al*. *In situ* bioprinting: Tailored printing strategies for regenerative medicine. *Int J Bioprint*. 2024;10(5):3366. doi: 10.36922/ijb.3366

38. Ashammakhi N, Ahadian S, Pountos I, *et al*. *In situ* three-dimensional printing for reparative and regenerative therapy. Biomed Microdevices. 2019;21(2):42. doi: 10.1007/s10544-019-0372-2

39. Wang MY, He JK, Liu YX, *et al*. The trend towards *in vivo* bioprinting. *Int J Bioprinting*. 2015;1(1): 15–26. doi: 10.18063/IJB.2015.01.001

40. Chaudhry MS, Czekanski A. *In-situ* bioprinting of skin - a review. *Bioprinting*. 2023;e00271:1-15. doi: 10.1016/j.bprint.2023.e00271

41. Wallace HA, Basehore BM, Zito PM. Wound healing phases. In: StatPearls [Internet]. Treasure Island (FL): StatPearls Publishing; 2025.

42. Zhu W, Nie X, Tao Q, Yao H, Wang DA. Interactions at engineered graft-tissue interfaces: a review. *APL Bioeng.* 2020;4(3):031502. doi: 10.1063/5.0014519

43. Kuffler DP. Photobiomodulation in promoting wound healing: a review. *Regen Med.* 2016;11(1):107-22. doi: 10.2217/rme.15.82

44. Mosca RC, Ong AA, Albasha O, Bass K, Arany P. Photobiomodulation therapy for wound care: a potent, noninvasive, photoceutical approach. *Adv Skin wound care*. 2019;32(4):157-167. doi: 10.1097/01.ASW.0000553600.97572.d2